



# Temporal and Latitudinal Variations in Ca-K Plage and Network Area: An Implication for Meridional Flows

Muthu Priyal , Jagdev Singh , Belur Ravindra , and G. Sindhuja

Indian Institute of Astrophysics, Bangalore, India; [ravindra@iiap.res.in](mailto:ravindra@iiap.res.in)

Received 2022 June 20; revised 2022 November 5; accepted 2022 December 30; published 2023 February 28

## Abstract

The Ca-K spectroheliograms obtained at the Kodaikanal observatory are used to generate a uniform time series using the equal-contrast technique for studying the long- and short-term variations in the solar chromosphere. The percentages of plage, enhanced network, and active and quiet network areas at various latitudes is compared with the activity at  $35^\circ$  latitude and also with the sunspot number for the period of 1907–1984. The values of the phase differences indicate that the activity begins at  $\sim 45^\circ$  latitude and shifts progressively to a lower latitude at a speed of  $\sim 9.4 \text{ m s}^{-1}$ . The shift speed slows down gradually and reaches  $\sim 3 \text{ m s}^{-1}$  at  $\sim 5^\circ$  latitude. No phase difference between the variations of Ca-K activity at  $55^\circ$ ,  $65^\circ$ , and  $75^\circ$  latitude belts implies that changes in the activity are happening simultaneously. The analysis shows that the activity at polar latitude belts is anticorrelated with the sunspot number. This study indicates that a multicell meridional flow pattern could exist in the latitude direction. One type of cell could transport the magnetic elements from mid- to low-latitude belts through meridional flows, and the other cell type could be operating in the polar region.

*Unified Astronomy Thesaurus concepts:* [Solar cycle \(1487\)](#); [Plages \(1240\)](#); [Solar activity \(1475\)](#)

## 1. Introduction

Almost all the variations on the Sun are related to the growth and decay of the active regions on the Sun. The existence of the solar cycle was discovered by Schwabe (1843) from the variations in the sunspot number over 11 yr. The sunspots appear at midlatitudes during the beginning of the cycle and then appear at lower and lower latitudes with time.

Hale (1908) found that sunspots are regions in which the magnetic field is high. Babcock (1961) proposed that the differential rotation of the Sun generates a toroidal field and that the decay of sunspots results in the generation of a poloidal field that shifts toward the northern and southern poles of the Sun. The meridional flow governs the pattern of the sunspot occurrence on the Sun. Howard & Labonte (1981) suggested that the formation of the polar field is due to the migration of weak magnetic fields toward the poles. A poleward migration of the weak magnetic field was also reported by Wang & Sheeley (1988), Cameron & Hopkins (1998), and Durrant et al. (2004). Ananthakrishnan (1952) reported the movement of prominences from midlatitudes toward the poles. Hathaway (2003) discussed the role of the equatorward meridional flow in transporting the toroidal component of the magnetic field. Modeling of the solar dynamo (Dikpati & Gilman 2006; Dikpati et al. 2010) has shown the importance of the meridional flow pattern for understanding the solar cycle.

The systematic large-scale plasma flows from the equator toward the poles just below the solar surface and from the poles toward the equator deep inside the Sun plays a vital role in the solar magnetic dynamo (Choudhuri et al. 1995; Charbonneau et al. 2007; Nandy et al. 2011). Meridional flow studies made using magnetic field observations indicated that during solar minimum, the magnetic field peaked at the polar region

(Wang & Sheeley 1988). Worden & Harvey (2000) pointed out that measurements of a flux distribution beyond  $75^\circ$  latitude are significantly uncertain because of canopy effects and the geometrical foreshortening of features. Raouafi et al. (2007) found that the field strength remains flat between latitudes  $55^\circ$  and  $75^\circ$  and then decreases by more than 50% in the polar region. With the feature-tracking technique, the meridional flow speed on the solar surface has been found to be between  $10$  and  $20 \text{ m s}^{-1}$  toward the pole (Komm et al. 1993; Hathaway & Rightmire 2010). Zhao et al. (2013) reported a poleward flow with a velocity of  $15 \text{ m s}^{-1}$  and an equator-ward flow in the middle of the convection zone, suggesting a double-cell meridional flow profile. In contrast, a detailed data analysis by Rajaguru & Antia (2015) suggests a single-cell meridional circulation.

Leighton (1959) reported that the Ca-K plage regions have a magnetic field between 100 and 200 Gauss and a Ca-K intensity related to the strength of the magnetic field. Leighton (1964) showed that the pattern of Ca-K network cells resembles the boundaries of large convective cells seen in photospheric dopplergrams. Furthermore, Sivaraman & Livingston (1982) found that Ca-K bright points and weak magnetic field regions are cospatial and that the bright region changes its location with the movement of an associated magnetic field. Thus, the variations in Ca-K features or flux can be used to understand the solar dynamo because of the correlation between the Ca-K line and the magnetic field regions at all length and strength scales on the Sun (Skumanich et al. 1975; Ortiz & Rast 2005).

Sindhuja et al. (2014) analyzed the spectra obtained at Kodaikanal Observatory (KO) as a function of latitude, integrated over the visible longitudes for 1989–2011. The details of observations and the initial analysis are given in Singh (1988) and Singh et al. (2004). The increase in  $K_1$  and decrease in the width of  $K_2$  indicates an increase in Ca-K emission, implying an increase in activity (White & Livingston 1981; Sivaraman et al. 1987). Sindhuja et al. (2014) and

Sindhuja et al. (2015) found that the  $K_1$  and  $K_2$  widths of the Ca-K line varied at all latitudes with an 11 yr period, but the maximum of the  $K_1$  width occurred at different times at different latitude belts. The  $K_1$  width varied by  $\sim 30\%$  at the equatorial belts, but by only  $\sim 6\%$  at latitude belts around  $50^\circ$ . The variations in the width of  $K_1$  in the polar region are anticorrelated with the variation at the  $35^\circ$  latitude belt with a phase difference of about 5 yr, in agreement with the findings of Makarov et al. (2004). From the phase difference at different latitude belts with respect to the  $35^\circ$  belt, Makarov and collaborators found that during the beginning of the solar cycle, the activity shifted from midlatitude toward the equator with a speed of  $\sim 5 \text{ m s}^{-1}$  in the northern and  $\sim 14 \text{ m s}^{-1}$  in the southern hemisphere.

Following these investigations, Devi et al. (2021) selected  $\sim 22960$  out of 34453 corrected images to identify Ca-K line features such as plage, enhanced network (EN), and active and quiet network (AN and QN) areas integrated over  $10^\circ$  latitude belts by using the intensity and area threshold values. Due to significant data gaps, the resulting parameters were averaged over a month with a running average over three years. Considering the data of nine solar cycles, they found that activity shifts from midlatitude toward the equator at a faster speed at the beginning of the solar cycle. The speed decreases as the cycle progresses. The average speed of the activity shift varied between  $\sim 19$  and  $3 \text{ m s}^{-1}$  from 1913 to 2004.

Singh et al. (2021) have rescaled the Ca-K spectroheliograms (KO) using the equal-contrast technique (ECT) to generate a more uniform time series consisting of all the 34453 images taken over 16981 days during the period 1905–2007. There are fewer gaps in the data than in the time series used by Devi et al. (2021). We have analyzed this time series as a function of latitude to study the variation of plage, EN, AN, and QN areas with time. In this article, we report the variations in the Ca-K parameters with a better accuracy with averaged parameters over a shorter period. We computed the speed of the activity shift from midlatitude toward equator and poles for each solar cycle from 1905 to 2004.

## 2. Data Analysis

The Ca-K spectroheliograms were obtained daily at KO from 1905 to 2007, with a few gaps due to sky conditions and instrument problems. These images were digitized with a pixel resolution of  $0''.86$  and 16 bit readout using a CCD detector of  $4\text{K} \times 4\text{K}$  format. The digitized images were calibrated, and a long time series of equal-contrast images was generated by causing the full width at half maximum (FWHM) of the normalized intensity distribution to lie between 0.10 and 0.11 (Priyal et al. 2019; Singh et al. 2021). The first and second columns of Figure 1 show the images with high (quiet phase,  $\text{FWHM} = 0.231$ ), low (active phase,  $\text{FWHM} = 0.068$ ), and intermediate contrast ( $\text{FWHM} = 0.096$ ) and the normalized intensity distribution of these images, respectively. In the histograms, the area below the curve with an intensity  $> 1.1$  is the indicator of Ca-K active regions. This area for the quiet phase exceeds that for the active phase, in contrast to expectation. This is because of the difference in the contrast of these images. The third and fourth columns of the figure show the images and their intensity distribution after applying the ECT procedure. The FWHM values of the intensity distribution become similar after the

ECT application for all the images, and hence their contrast becomes similar.

We segregated Ca-K features such as plages, EN, AN, and QN regions based on the intensity and area threshold. Then, we defined the plage area as regions on the Sun having a normalized intensity  $> 1.30$ , an area of consecutive pixels  $> 500$ , and an EN with an area  $> 10$  and  $< 500$  pixels. Five hundred pixels are equivalent to  $370 \text{ arcsec}^2$ , which is about half the size of a large convective cell, and 10 pixels correspond to  $7.4 \text{ arcsec}^2$ . The threshold values for AN have been defined as regions with an intensity  $> 1.20$  and  $< 1.30$  with a size  $> 10$  pixels, and the thresholds for QN are an intensity  $> 1.10$  and  $< 1.20$  with an area of 5 pixels, which is equivalent to  $3.7 \text{ arcsec}^2$ ; this is slightly larger than the size of a granule. Generally, the width of the network boundary is about  $8''$ , which is equal to 10 pixels (Singh & Bappu 1981). Therefore, we decided on a minimum number of pixels to identify EN, AN, and QN to avoid the contribution from groups of only a few pixels that may not be part of a Ca-K active region. Considering the radius of the observed image and the B angle of the Sun on the day of observations, we prepared the solar grid with an interval of  $10^\circ$  in latitude up to  $90^\circ$ . The areas of different Ca-K features are determined in each segment using the intensity and area threshold values. After analyzing all images, we derived the average values of the Ca-K parameters when multiple images were available on a single day. We have used the Ca-K data for the period 1907–84 to study the phase differences in the variation of active areas at various latitudes.

To see how well the solar mean magnetic field and overall Ca-K brightenings are correlated, we used the magnetic field records of the Wilcox Solar Observatory (WSO).<sup>2</sup> We plot the measured values of Ca-K active area (integrated area over all latitudes) versus magnetic field (Figure 2) for the period 1975–84, which shows a good agreement between the two parameters with a correlation coefficient of 0.60.

Like any other ground-based observatory, KO also receives monsoon rains between June and October. During this period, the number of days with a clear sky is smaller. The upper panel of Figure 3 shows the histograms of the number of images per year that are available in the Ca-K time series. The bottom panel of the figure indicates the number of days per year when observations were made. Generally, observations could be made on  $> 250$  days per year until 1957 and on  $> 200$  days per year from 1958 to 1983, restricted mainly by the sky conditions. The number of images reduced to  $< 150$  per year from 1984 to 2007. This is because of the weather, the working condition of the instrument, and the availability of photographic films. No observations could be obtained on some of the days because of gaps in the data. The derived values of plage, EN, AN, and QN areas were interpolated using the IDL subroutine Interpol.pro for the nonavailability of data on these days by considering the values adjacent to the gap.

There are numerous small-scale features found at each latitude belt. We therefore did not apply the correction for the foreshortening effect to the area of the detected features. We just computed the total area of plage and small-scale features at each latitude belt of  $10^\circ$  each. To account for the different areas at each latitude belt, we determined the fractional area of each feature by considering the total area of that latitude belt. Then, we determined the time difference between the occurrences of a

<sup>2</sup> <http://wso.stanford.edu/#MeanField>

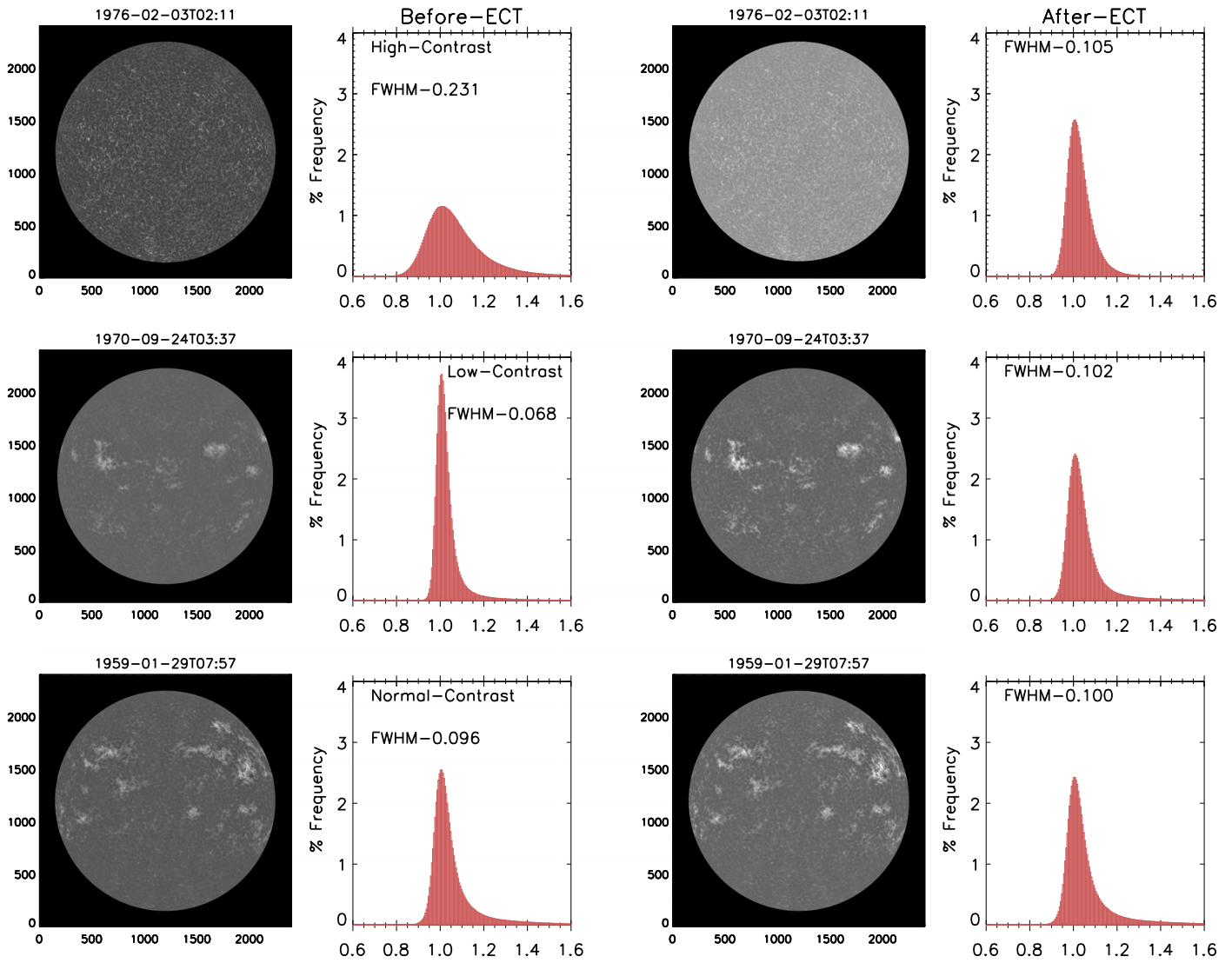


**Figure 1.** Four panels in the first row of the figure show the image before the ECT application, its intensity distribution, the image after the ECT procedure, and its intensity distribution for a high-contrast image obtained during quiet phase of the Sun. The FWHM of the intensity distribution is indicated in each panel of the intensity distribution. The middle and bottom row show the same for the low- and normal-contrast images, respectively.

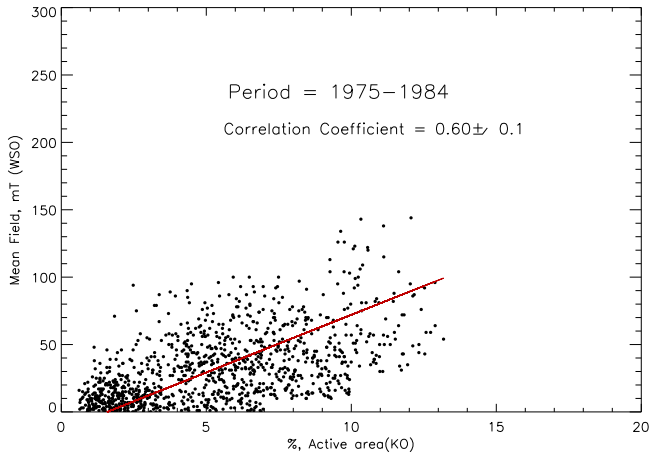


**Figure 2.** Scatter plot of the mean magnetic field measured at WSO vs. the percentage of the Ca-K active area.

maximum of each feature in the time series at different latitude belts with respect to the  $35^\circ$  latitude belt by employing the cross correlation between the two.

Similarly, we computed the time difference between the peaks of Ca-K features in the time series of data at different latitude belts with respect to the sunspot number on the whole disk as a reference. Considering the radius and circumference of the Sun at zero-degree longitude, the surface distance between the centers of any two latitudes separated by  $10^\circ$  is 121475 km, regardless of the latitude. Thus, the phase difference of one month between two latitudes yields a velocity of  $47 \text{ m s}^{-1}$  on the solar surface. The velocity is computed using the distance in meters on the solar surface divided by the phase difference in seconds, thus, making it independent of the spherical geometry of the Sun. We are computing the speed of shift in the latitude direction. Therefore, the movement along the longitudinal direction due to spherical geometry may not affect the results.

### 3. Results

We study the variation in the detected fractional plage area and small-scale feature (EN, AN, and QN) with time at various latitudes at an interval of  $10^\circ$  up to the  $80^\circ$  latitude belts.

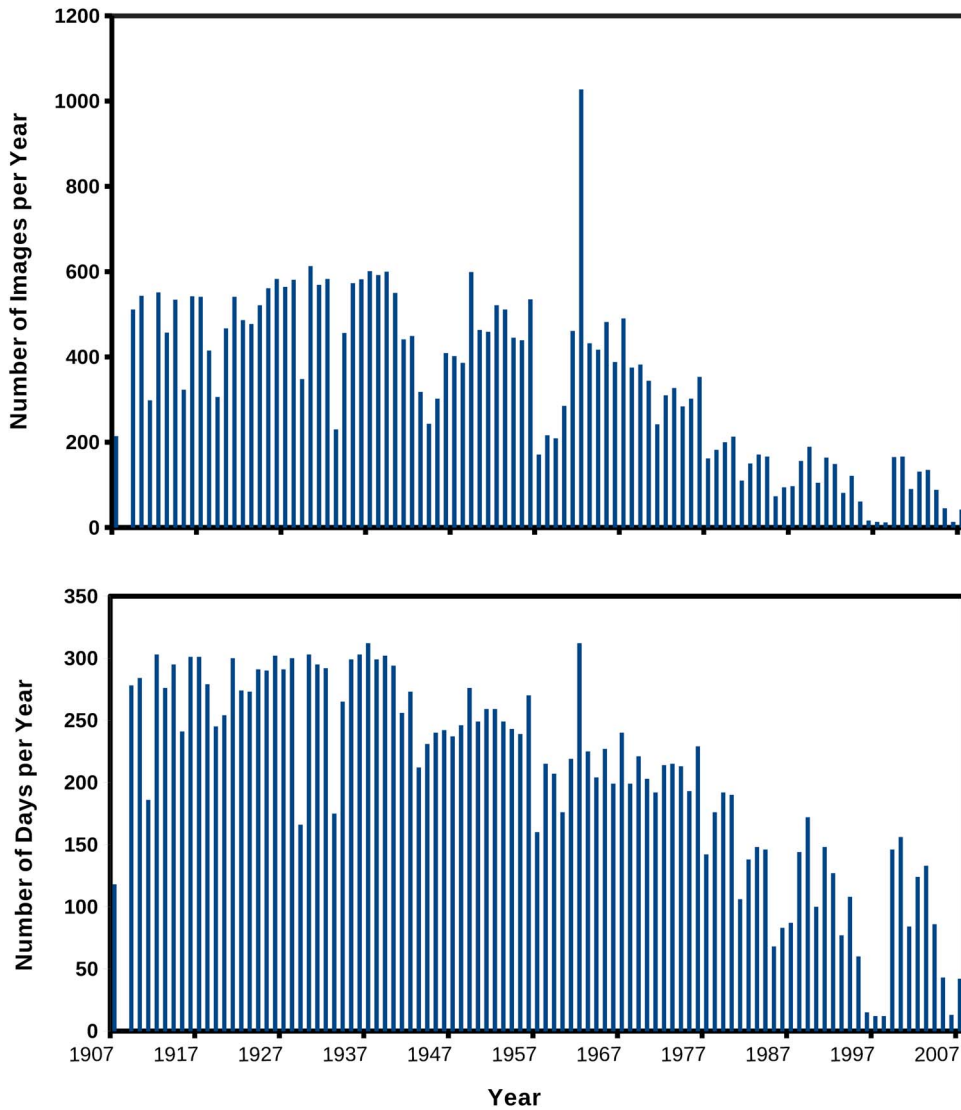


**Figure 3.** Upper panel: number of images per year obtained at KO during the period 1907–2007. Lower panel: observations made on a number of days per year.

Sunspots appear at  $\sim 35^\circ$  latitudes at the beginning of the solar cycle. Therefore, we determine the speed of the activity shift by computing the phase difference between the occurrences of maximum activity at various latitudes with respect to that at the  $35^\circ$  latitude belt.

### 3.1. Latitudinal Variation in the Fractional Plage Area with Time

To study the variation in the plage area with time, we have computed the fractional area in each latitude belt, considering the area of that latitude belt. Monthly averages are computed using the daily data. Then these values were smoothed by taking the running average over three months to study the long-term variations. In the five panels of Figure 4, we show the fractional plage area on a monthly basis for  $0^\circ$ – $10^\circ$ ,  $10^\circ$ – $20^\circ$ ,  $20^\circ$ – $30^\circ$ ,  $30^\circ$ – $40^\circ$ , and  $40^\circ$ – $50^\circ$  northern latitude belts in red. In blue we show the areas for the southern belts for the period of 1907–2007. The latitude belt is indicated in each panel. Hereafter, we refer to them by the mean latitude as  $5^\circ$ ,  $15^\circ$ ,  $25^\circ$ ,  $35^\circ$ , and  $45^\circ$  latitude belts. The sunspot number representing the whole solar disk with the same averaging procedure is shown in black. The comparison of the variations in Ca-K

plage area at  $25^\circ$  and  $35^\circ$  latitude belts with sunspot number on the disk indicates that the maximum Ca-K plage area occurs at these belts before the sunspot maximum, whereas at the  $5^\circ$  belt, it happens after the sunspot maximum. It appears that the phase difference between sunspot numbers and fractional plage area at the  $15^\circ$  belts is minimum. We have plotted the fractional plage area up to  $50^\circ$  latitude belts, as these belts are rarely seen at higher latitudes. The variations in the small-scale Ca-K features such as EN, AN, and QN are similar to the plage variations. The details of the variations in small-scale features are shown in Appendix A.

### 3.2. Phase Difference between Activities at Different Latitude Belts

To determine the speed of the activity shift in the Sun as a function of latitude, we computed the phase difference using monthly data. We used a cross-correlation analysis to determine the phase shift in the activity between the latitudes in steps of one month from  $\pm 1$  to 100 months. Generally, the active regions first appear around  $35^\circ$  latitude at the beginning of a solar cycle. As the cycle progresses, the plages (representing the toroidal magnetic field) gradually appear at

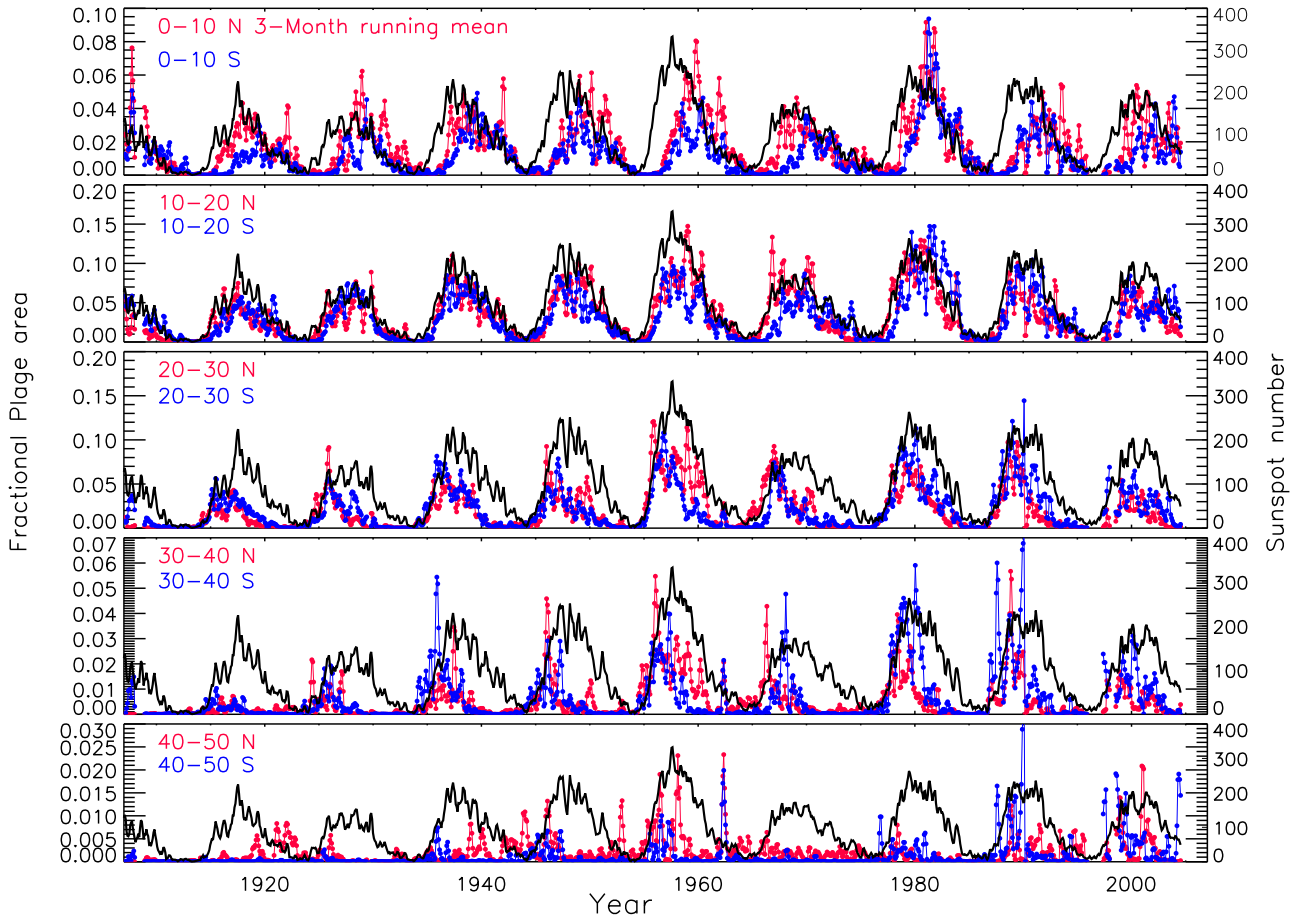


**Figure 4.** Five panels show the monthly variation in fractional plate area with a three-month running-average basis for the period 1907–2007 for the equatorial belts ( $5^{\circ}$ – $45^{\circ}$ ) at an interval of  $10^{\circ}$  for the northern (red) and southern (blue) hemispheres. Sunspot data with the same averages but for the whole Sun are overplotted for comparison. The latitude belt is indicated in each panel.

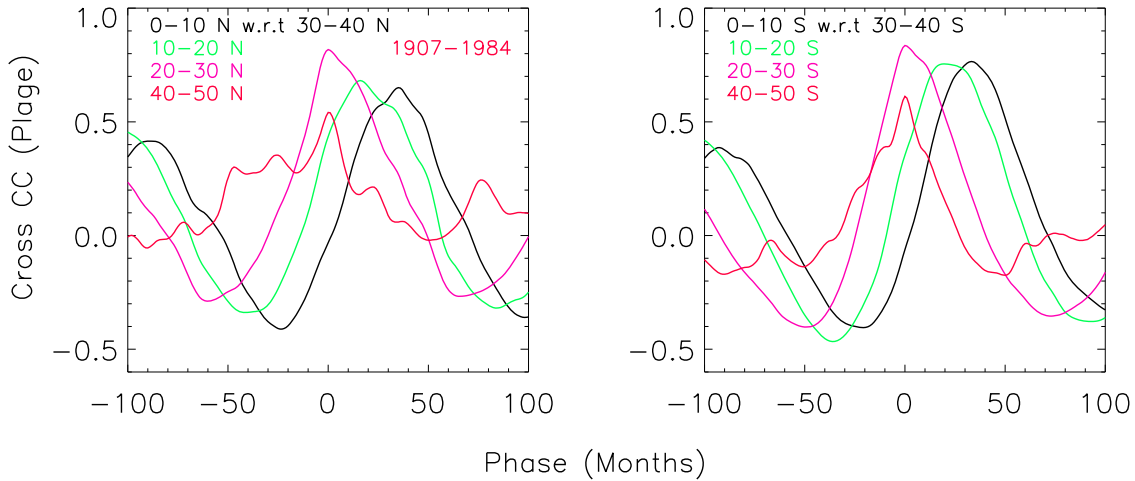


**Figure 5.** Cross-correlation curves for the  $5^{\circ}$  (black),  $15^{\circ}$  (green),  $25^{\circ}$  (pink), and  $45^{\circ}$  (red) latitude with respect to the  $35^{\circ}$  latitude for Ca–K plate area considering the period of 1907–1984.

lower latitudes. Therefore, to estimate the speed of the shift, we computed the phase difference for various latitude belts with the  $35^{\circ}$  belt. We used the monthly fractional area with a running average over 13 months to determine the phase difference. Two panels of Figure 5 show the cross-correlation values of  $5^{\circ}$ ,  $15^{\circ}$ ,  $25^{\circ}$ , and  $45^{\circ}$  latitude belts with respect to the  $35^{\circ}$  belt for the fractional plate area for the southern and northern hemispheres considering the data for the period

1907–1984 together. The data for the period 1985–2007 were not considered because of significant gaps in the observations.

The two panels in the upper row of Figure 6 show the cross-correlation function for the  $5^{\circ}$ ,  $15^{\circ}$ ,  $25^{\circ}$ , and  $45^{\circ}$  belts with respect to the  $35^{\circ}$  belt for the fractional EN area for the two hemispheres. The two panels in the bottom row indicate the cross-correlation function for the  $55^{\circ}$ ,  $65^{\circ}$ , and  $75^{\circ}$  belts with the  $35^{\circ}$  belt. We also computed the cross-correlation values for

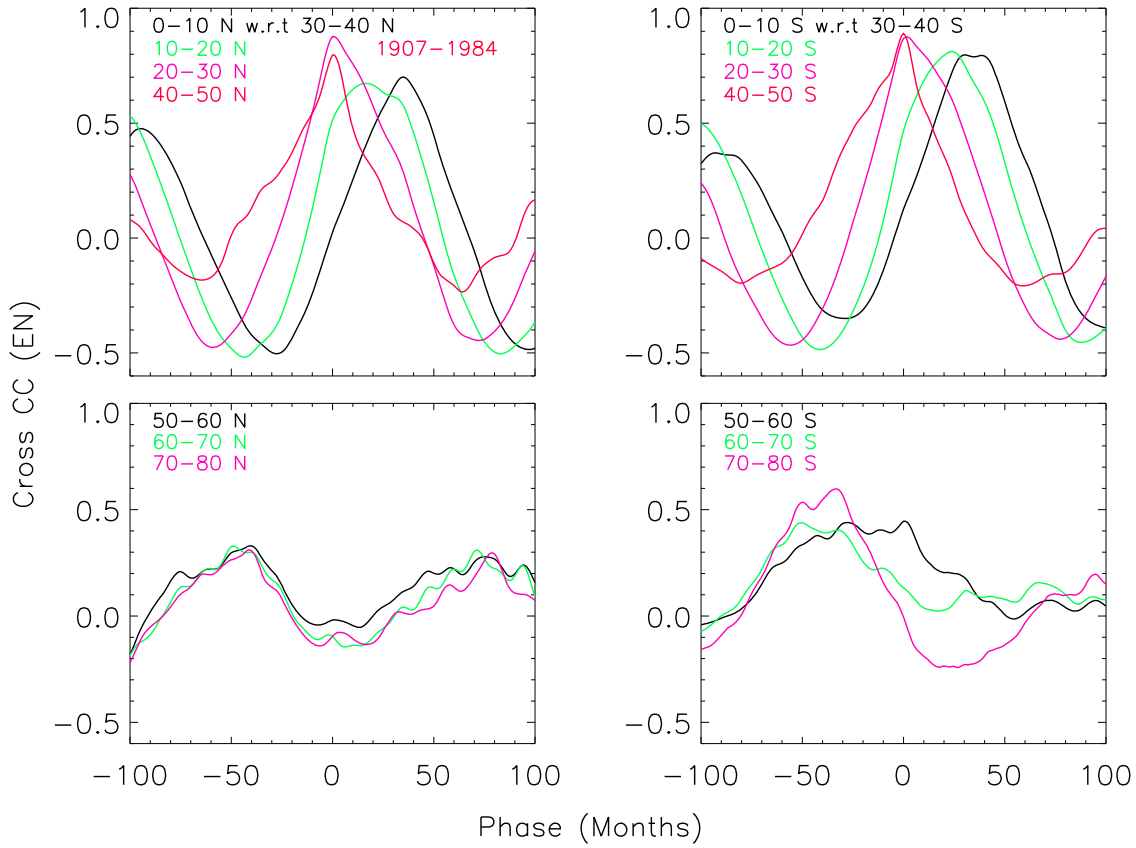


**Figure 6.** Cross-correlation curves for various latitude belts with respect to the 35° latitude belt for the EN area considering the data for the period of 1907–84.

**Table 1**

Values of the Cross Correlation and Phase Difference for Plage, EN, AN, and QN for Various Latitude Belts with Respect to the 35° Belt Considering the Period of 1907–84

Cross Correlation between Latitudes	Maximum Value—Cross-correlation				Phase Difference in Months			
	Coefficients							
	Plage	EN	AN	QN	Plage	EN	AN	QN
05°–35° N	0.65	0.7	0.70	0.46	37	36	35	35
15°–35° N	0.86	0.67	0.74	0.67	18	22	21	19
25°–35° N	0.82	0.88	0.90	0.90	7	10	9	5
35°–35° N	1	1	1	1	0	0	0	0
45°–35° N	0.54	0.80	0.70	0.76	–4	–6	–5	–4
55°–35° N	NSP	0.33,0.28	0.33,0.35	NSP	NSP	–51, 72	–54, 70	NSP
65°–35° N	NSP	0.32,0.33	0.29,31	NSP	NSP	–53, 63	–56, 67	NSP
75°–35° N	NSP	0.30,0.32	0.33,31	NSP	NSP	–50, 68	–50, 72	NSP
05°–35° S	0.76	0.80	0.81	0.64	34	35	37	41
15°–35° S	0.75	0.81	0.79	0.68	19	23	24	21
25°–35° S	0.85	0.87	0.88	0.84	6	9	8	5
35°–35° S	1	1	1	1	0	0	0	0
45°–35° S	0.61	0.89	0.82	0.81	–5	–6	–3	–2
55°–35° S	NSP	0.45	0.32,0.28	0.54,0.22	NSP	–34	–42, 7	–33, 73
65°–35° S	NSP	0.44	0.47,0.34	0.45,0.24	NSP	–46	–38, 75	–35, 74
75°–35° S	NSP	0.60	0.45,0.26	0.44, NSP	NSP	–42	–45, 71	–34, NSP

**Note.** “NSP” indicates when no significant peak is found in the cross-correlation curve.

the fractional AN and QN for all the belts. The results for AN and QN are similar to those for EN and the plage areas. We also computed the phase difference between the activity at different latitudes for individual solar cycles. The results are discussed in Appendix B.

The occurrences of peaks and valleys of small-scale structures (networks) in the time series follow the variation in large-scale features, such as sunspots and plages. The plage areas represent the large-scale toroidal field, and networks refer to poloidal fields. Hereafter, we refer to this temporal variation

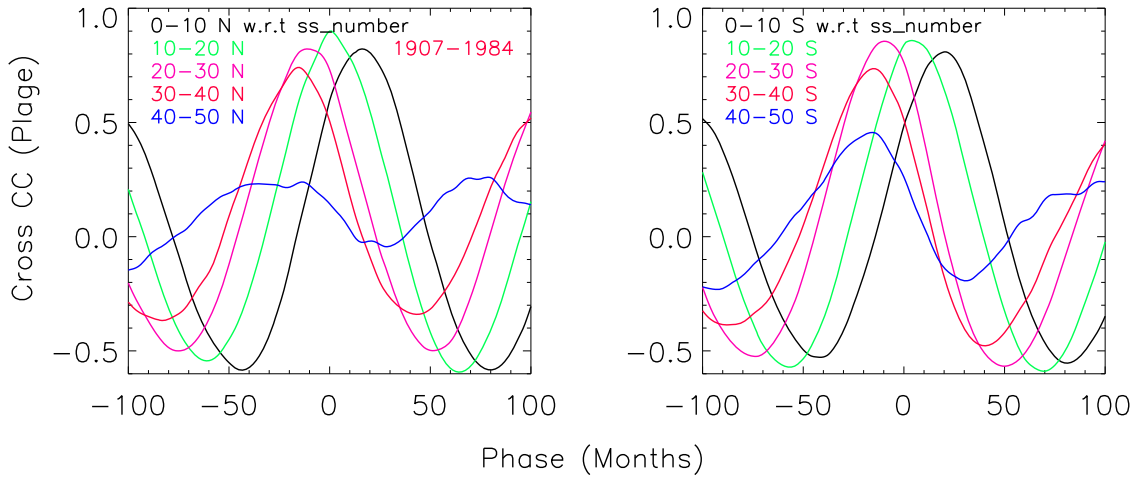


**Figure 7.** Cross-correlation curves of the Ca–K plage area for the 5°, 15°, 25°, 35°, and 45° latitude belts with respect to SS over the visible disk considering the period of 1907–1984.

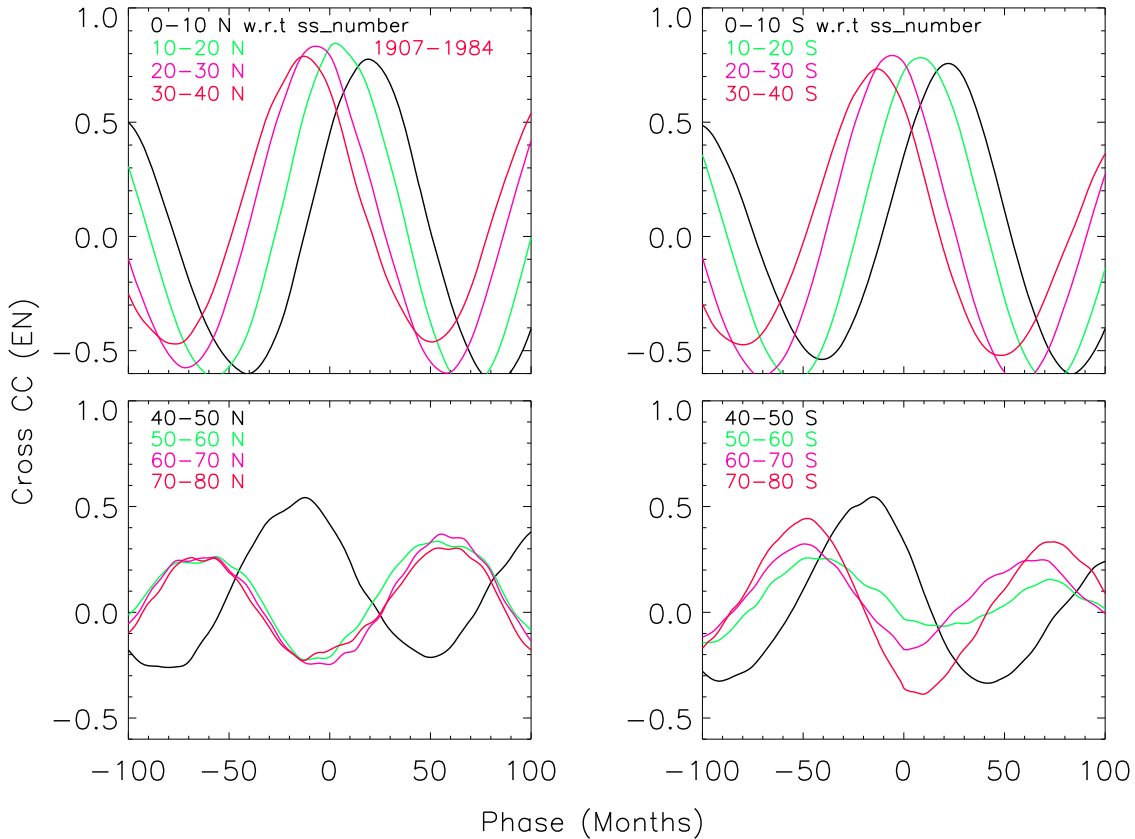


**Figure 8.** Cross-correlation curves of Ca–K EN area for the 5°, 15°, 25°, 35°, and 45° latitude belts with respect to SS over the visible disk considering the period of 1907–1984.

in plage and network areas as “activity.” It may be noted that plages only occur up to  $\sim 50^\circ$ , whereas networks are visible on the whole solar surface. While discussing the polar region, we only imply small-scale features (networks). The phase difference between the two latitude belts gives the time difference between the occurrences of the maximum area (peak) of activity at the two latitude belts. The values of the amplitude of the cross-correlation coefficient and phase difference in months for various latitude belts with respect to

the  $35^\circ$  latitude are listed in Table 1. The negative phase (Table 1) difference between the  $45^\circ$  and  $35^\circ$  latitude belts implies that the maximum area of the networks at the  $45^\circ$  belt occurred earlier than that at the  $35^\circ$  belt. The values of the phase difference for different latitude belts imply that the shift speed of the activity at the beginning of the solar cycle is higher than near the end of the cycle. The difference in time for the occurrence of maximum activity at  $35^\circ$  and  $5^\circ$  is about 36 months in both hemispheres.

**Table 2**

Values of the Phase Differences for Plage, EN, AN, and QN for Various Latitude Belts with Respect to SS over the Visible Solar Disk Considering the Period of 1907–84

Cross Correlation between Latitudes with SS	Phase Difference in Months for the Northern Hemisphere				Phase Difference in Months for the Southern Hemisphere			
	Plage	EN	AN	QN	Plage	EN	AN	QN
	05° –SS	18	20	18	16	20	21	22
15° –SS	1	3	3	1	3	7	5	5
25° –SS	–9	–7	–6	–8	–9	–7	–8	–7
35° –SS	–14	–12	–13	–13	–15	–13	–14	–14
45° –SS	–20	–15	–20	–18	–18	–16	–19	–17
55° –SS	NSP	–62, 54	–65, 56	–65, 56	NSP	–45, 73	–51, 68	–59, 70
65° –SS	NSP	–64, 56	–67, 60	–63, 59	NSP	–49, 70	–59, 63	–51, 65
75° –SS	NSP	–65, 52	–64, 62	–60, 64	NSP	–48, 75	–54, 70	–53, 71

**Note.** “NSP” indicates when no significant peak is found in the cross-correlation curve.

### 3.3. Phase Difference between Activities at Various Latitude Belts and Sunspot Number

The sunspot number is a good indicator of solar activity. For each cycle, the sunspot number attains a maximum value at a certain epoch that can be used as a reference to compute the phase difference between sunspot and Ca-K activities at different latitudes. We have computed the cross-correlation functions for the Ca-K features such as plage, EN, AN, and QN area with respect to sunspot numbers (SS) over the visible disk. The cross-correlation curves for the plage area are shown in Figure 7, and those for the EN area are plotted in Figure 8. The values of the phase differences between the occurrences of the area of Ca-K features at various latitudes and SS considering the data for the period 1907–84 are listed in Table 2. The correlation functions appear better and more consistent with the SS data than the Ca-K features at the 35° latitude belt. The correlation functions for the 55°–75° latitude belts are similar, showing almost the same phase difference with respect to SS for the high-latitude belts. The phase differences for individual cycles for EN and AN areas are given in Tables C1 and C2 (Appendix C) for the northern and southern hemispheres.

## 4. Discussion

We have computed the cross-correlation values between the activity at different latitude belts and at the 35° belt for up to 100 months on both sides of the zero-phase difference. The phase differences for the Ca-K line features such as plage, EN, AN, and QN with respect to corresponding activity at the 35° latitude belt show a similar trend for all the features and for all solar cycles. The values of the phase differences vary for each cycle, but it is difficult to say if they are of solar origin or within the statistical limits. Table 1 shows a positive phase difference for the 25°, 15°, and 5° latitude belts with respect to the 35° belts, but a negative phase difference between the 35° and 45° latitude belt. This implies that activity begins around the 45° latitude belt and then shifts to lower-latitude belts. The average values of the phase differences indicate that it takes about 5, 8, 12, and 16 months for the activity to travel from 45° to 35°, 35° to 25°, 25° to 15°, and 15° to 5°, respectively. This implies that the travel speed of the activity is  $\sim 9.6 \text{ m s}^{-1}$  at the beginning of the solar cycle at  $\sim 45^\circ$  latitude and decreases to  $\sim 3 \text{ m s}^{-1}$  near the end of the cycle at  $\sim 5^\circ$  latitude. The phase difference for the 55°, 65°, and 75° belts with respect to the 35° latitude belts remains the same.

We have also computed the cross correlation of the Ca-K features at different latitudes with respect to the SS on the visible disk. The average phase differences for all the features considering the data of 1907–84 indicate that it takes about 5, 6, 9, and 16 months for the activity to travel from 45° to 35°, 35° to 25°, 25° to 15°, and 15° to 5°, respectively, in the northern hemisphere, whereas it takes 4, 6, 13, and 16 months in the southern hemisphere. Comparatively, the activity took three months longer for the southern than for the northern hemisphere to travel from 45° to 5° latitude. The cross-correlation functions (Table 2) for the Ca-K features at the 65° and 75° belts with the SS show two peaks, one with a phase difference of  $\sim -5$ , and the other at  $+5$  yr. These two peaks are separated by 10–11 yr. Table 2 shows no systematic phase difference between the activity at 55°, 65°, and 75° latitudes.

The toroidal fields in the form of sunspots and plages appear at the solar surface around midlatitudes at the beginning of the solar cycle. They then occur at progressively lower latitudes as the cycle progresses (Babcock 1961). The poloidal component of the magnetic field moves toward the polar region with time. It may create variation in the small-scale activity at the polar latitude belt with time, caused by the dynamo process operating at the base of the convection zone of the Sun and meridional flows. There is a phase difference between the midlatitude and lower latitudes and between the midlatitude and polar latitudes. There are also minimum variations in the network areas at  $\sim 60^\circ$  latitude with the solar cycle as compared to other latitudes, including the polar region. These findings suggest that there could be two meridional circulation cells in the latitudinal direction, as suggested by Dikpati et al. (2010), Dikpati & Gilman (2012), and Belucz et al. (2015). One cell with a primary meridional flow is circulating from the equator up to 60° latitude. The second cell circulates in the other direction, from the poles toward 60° latitude. This makes the path shorter for magnetic flux transport through meridional circulation. The shorter path produces a shorter cycle with a period shorter than 11 yr. On the other hand, the Babcock (1961) and Leighton (1969) dynamo models suggest one meridional cell that runs from the equator to the poles and a return flow in the deep convection zone that can produce this effect. It may be noted that the occurrence of the maximum area of networks in the polar region is anticorrelated with that of the sunspot maxima (toroidal field) during the solar cycle, as reported by Makarov et al. (2004). Moreover, there is no



significant phase difference between the large- and small-scale activity at the middle- and lower-latitude belts.

### 5. Summary

Earlier, Singh et al. (2021, 2022) showed that the application of the ECT to the Ca-K images makes the data uniform and permits studying long-term variations in small-scale features reliably. Here, we demonstrated that plage, EN, AN, and QN areas could be used to study the variation in these features as a function of latitude and time, which has a direct bearing on the meridional flows generated by the dynamo at the base of the convection zone and just below the solar surface. We find that large-scale active regions appear on the solar surface at  $\sim 45^\circ$  latitude at the beginning of the solar cycle. The small-scale active areas also increase as the Ca-K plage areas increase at the respective latitude belts. The average value of the phase difference of five months between  $45^\circ$  and  $35^\circ$  (Table 1) indicates that the meridional flow has a velocity of about  $9.4 \text{ m s}^{-1}$  at the beginning of the solar cycle at the  $\sim 40^\circ$  latitude belt. Considering the average phase difference (plage and all networks) for the other latitude belts, we find that the speed decreases to  $\sim 6$ ,  $\sim 4.5$ , and  $\sim 3 \text{ m s}^{-1}$  at the  $25^\circ$ ,  $15^\circ$ , and  $5^\circ$  latitude belts, respectively. These are average values inferred from the phase differences in the occurrence of activity at these latitude belts. The cross-correlation function and phase differences indicate that the activity in the polar region is anticorrelated with the SS. There is no phase difference between the activity at the  $55^\circ$ ,  $65^\circ$ , and  $75^\circ$  latitude belts, raising doubt that the poloidal field moves from midlatitude belts to the polar region. These findings point toward the existence of multiple cells in the convection zone.

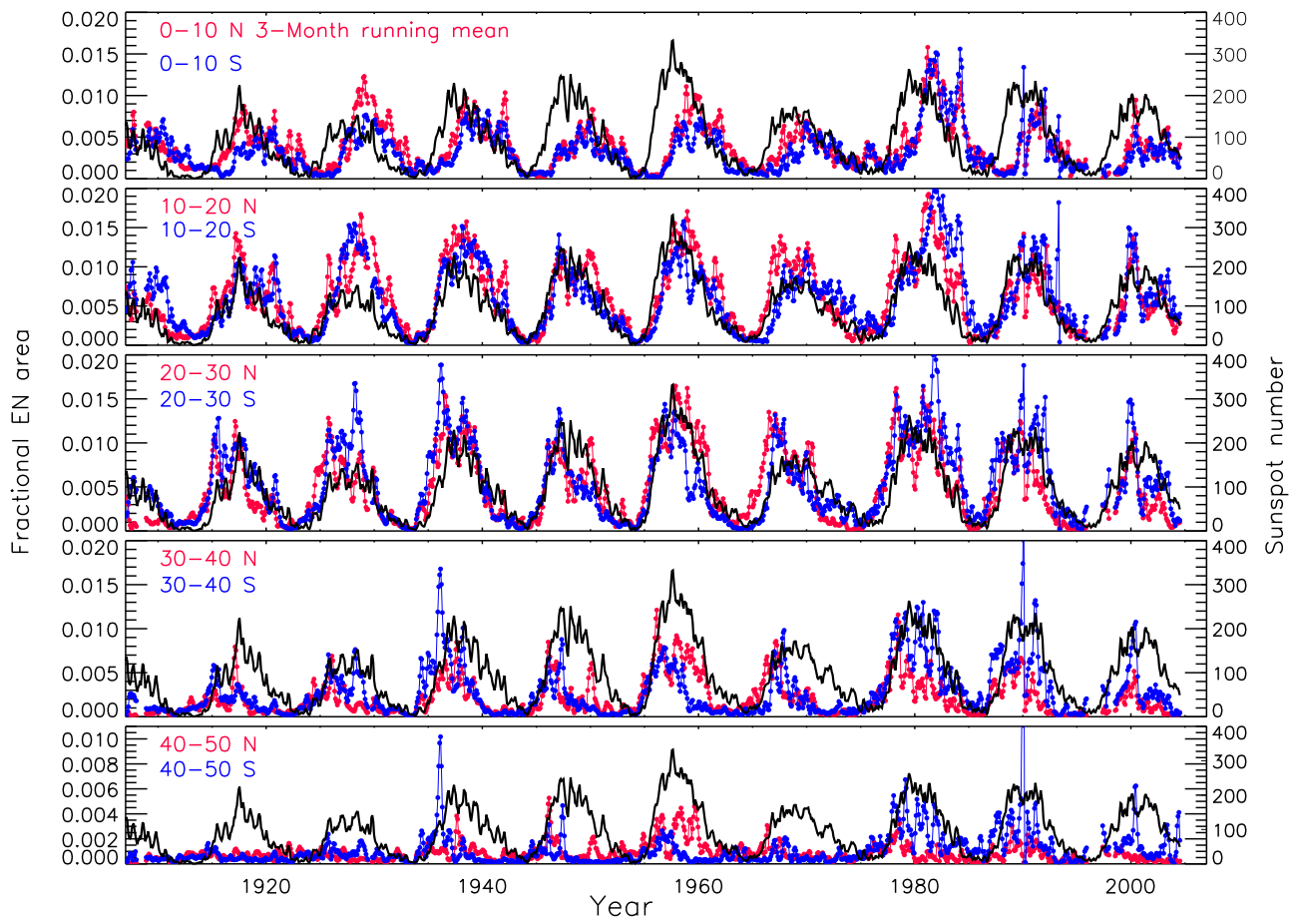
We thank the referee for the valuable comments. We thank the numerous observers who kept the data in good shape, and the digitization team for doing the laborious work. The digitization of the Kodaikanal solar data was planned by Jagdev Singh, and creation of the digitizers was supported by F. Gabriel and P U. Kamath.

## Appendix A Variations of Small-scale Ca-K Features with Time

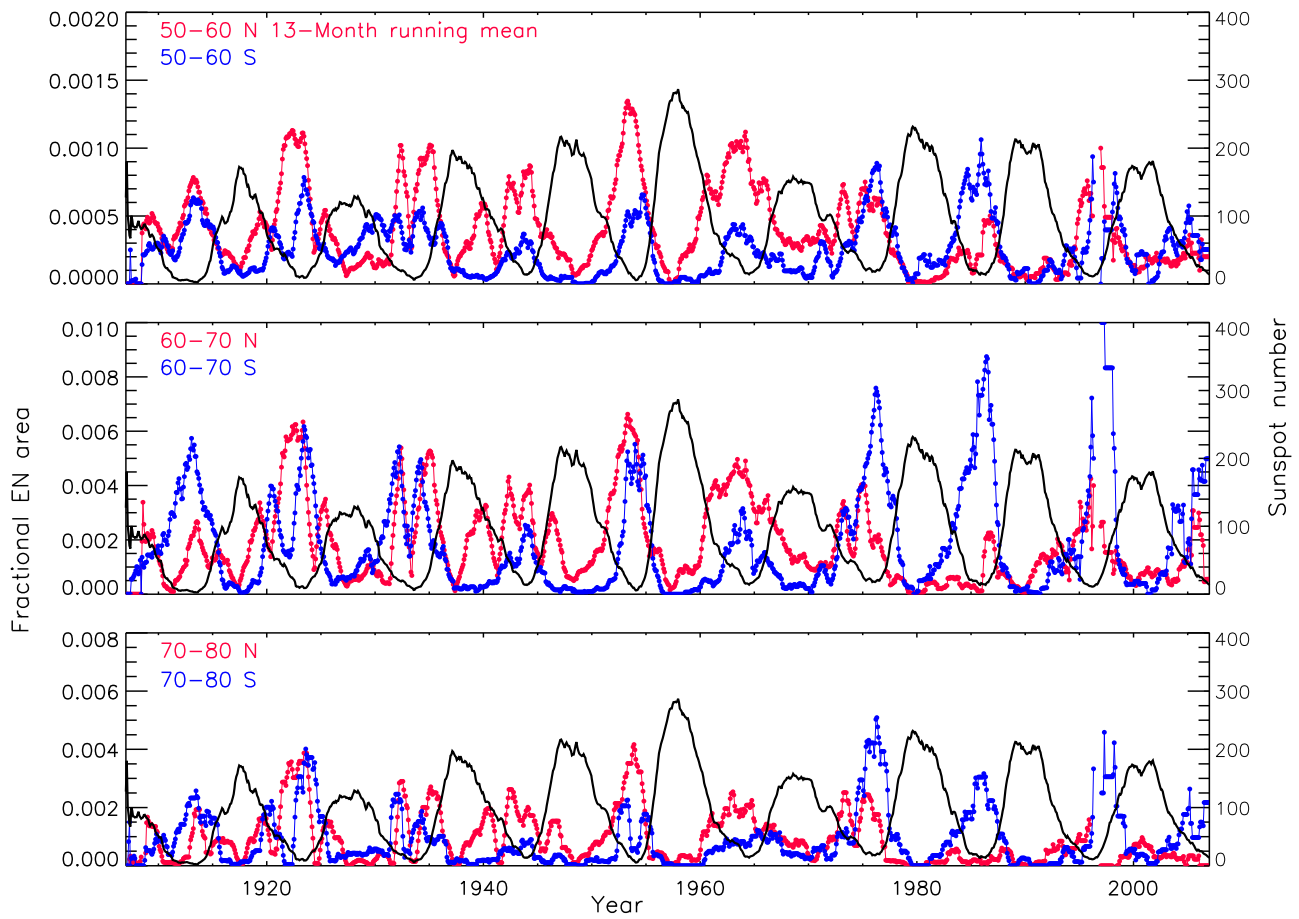
The variation in the plage area has been studied by many researchers over long periods, but the variation in small-scale Ca-K features (EN, AN, and QN) is investigated significantly less frequently due to the unavailability of properly calibrated images and due to the change in contrast of the images on a short- and long-term basis, as mentioned in the introduction. To study the long-term variation in the Ca-K features, we performed a monthly average of the data to reduce the effect of the solar rotational modulation. We again performed a three-month running average to suppress the remnant effects of rotation modulation.

Figure A1 shows the variation in fractional EN area as a function of time on a monthly basis with a running average over three months for the  $45^\circ$  south to  $45^\circ$  north latitudes at an interval of  $10^\circ$  for the period 1907–2007. Large-amplitude variations in the fractional EN area occur around the  $15^\circ$  latitude belts with the phase of the solar cycle as compared to other latitude belts. The variations at the  $15^\circ$  latitude belts also appear to be in phase with the sunspot cycle. The behavior of EN is similar to that of the plage area. Three panels of Figure A2 show the fractional EN area for the  $55^\circ$ – $75^\circ$  latitude belts for the two hemispheres in red (north) and blue (south) at an interval of  $10^\circ$  as a function of time on a monthly basis with a running average of 13 months. Figures A1 and A2 indicate that the fractional EN area at all latitude belts shows a periodicity of 11 yr.

Figures A3 and A4 show the fractional AN area variation at various latitude belts as a function of time with the same parameters as for the EN area. Figures A5 and A6 indicate the fractional QN variations on a monthly basis with the 13-month running average. All Figures A1–A6 show similar variations in EN, AN, and QN with varying amplitude as a function of feature and latitude. The small-scale features show 11 yr solar cycle variations up to the  $75^\circ$  latitude belts. Figures A2 for EN, A4 for AN, and A6 for QN area indicate that the occurrence of small-scale features in the polar region (latitude  $>65^\circ$ ) is anticorrelated with the SS.



**Figure A1.** Five panels show the monthly variation in fractional plage area on a three-month running average basis for the period 1907–2007 for the equatorial belts ( $5^{\circ}$ – $45^{\circ}$ ) at an interval of  $10^{\circ}$  for the northern (red) and southern (blue) hemispheres. Sunspot data with the same averages, but for the whole Sun, are overplotted for comparison. The latitude belt is indicated in each panel.



**Figure A2.** Three panels show the variation in fractional EN area with a 13-month running average for the period 1907–2007 for the polar latitude belts ( $55^{\circ}$ – $75^{\circ}$ ) at an interval of  $10^{\circ}$  for the northern (red) and southern (blue) hemispheres. Sunspot data with the same averages, but for the whole Sun, are overplotted for comparison. The latitude belt is indicated in each panel.

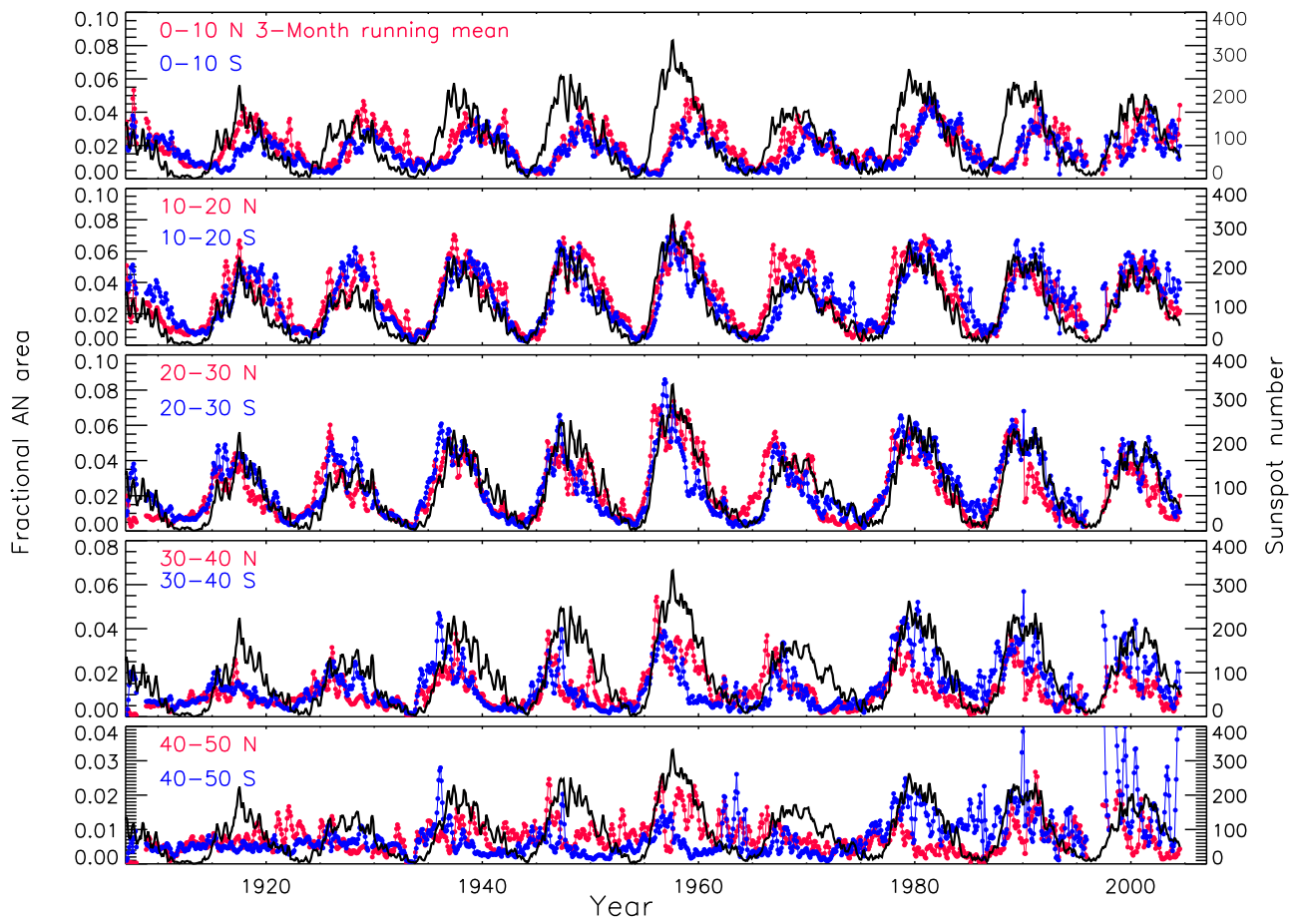
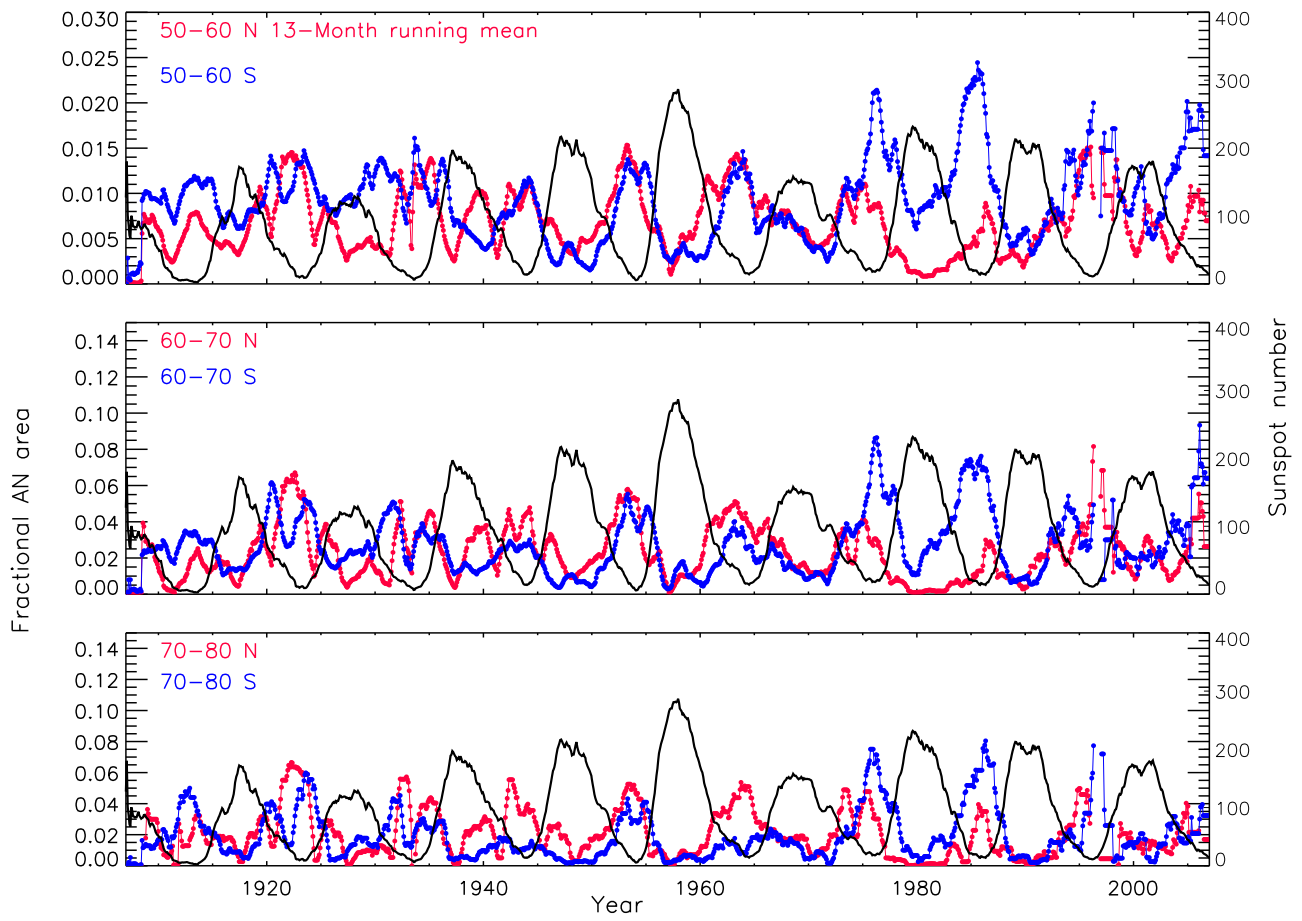


Figure A3. Same as for Figure A1, but for the fractional AN area.



**Figure A4.** Same as for Figure A2, but for the fractional AN area.

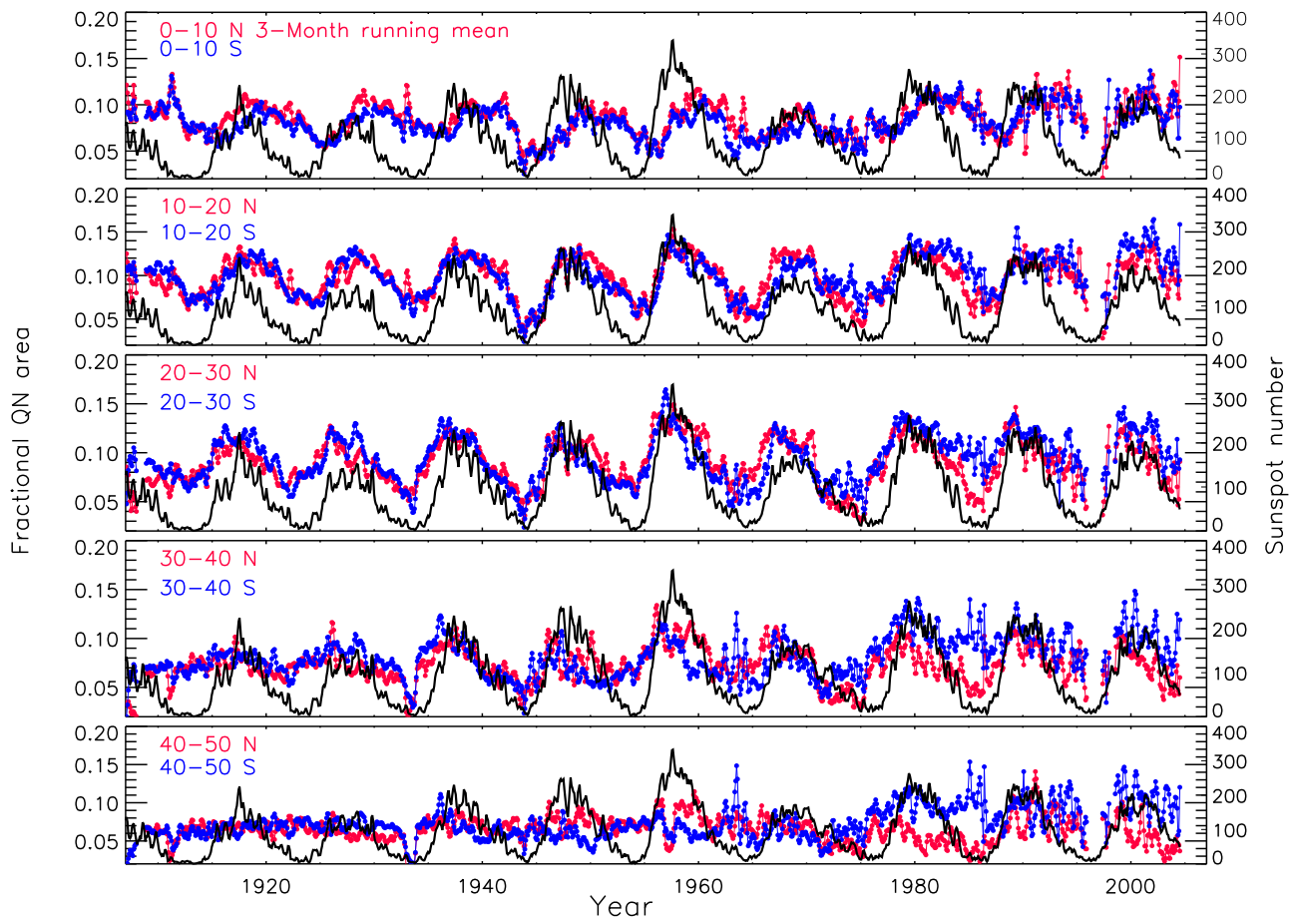


Figure A5. Same as for Figure A1, but for the fractional QN area.

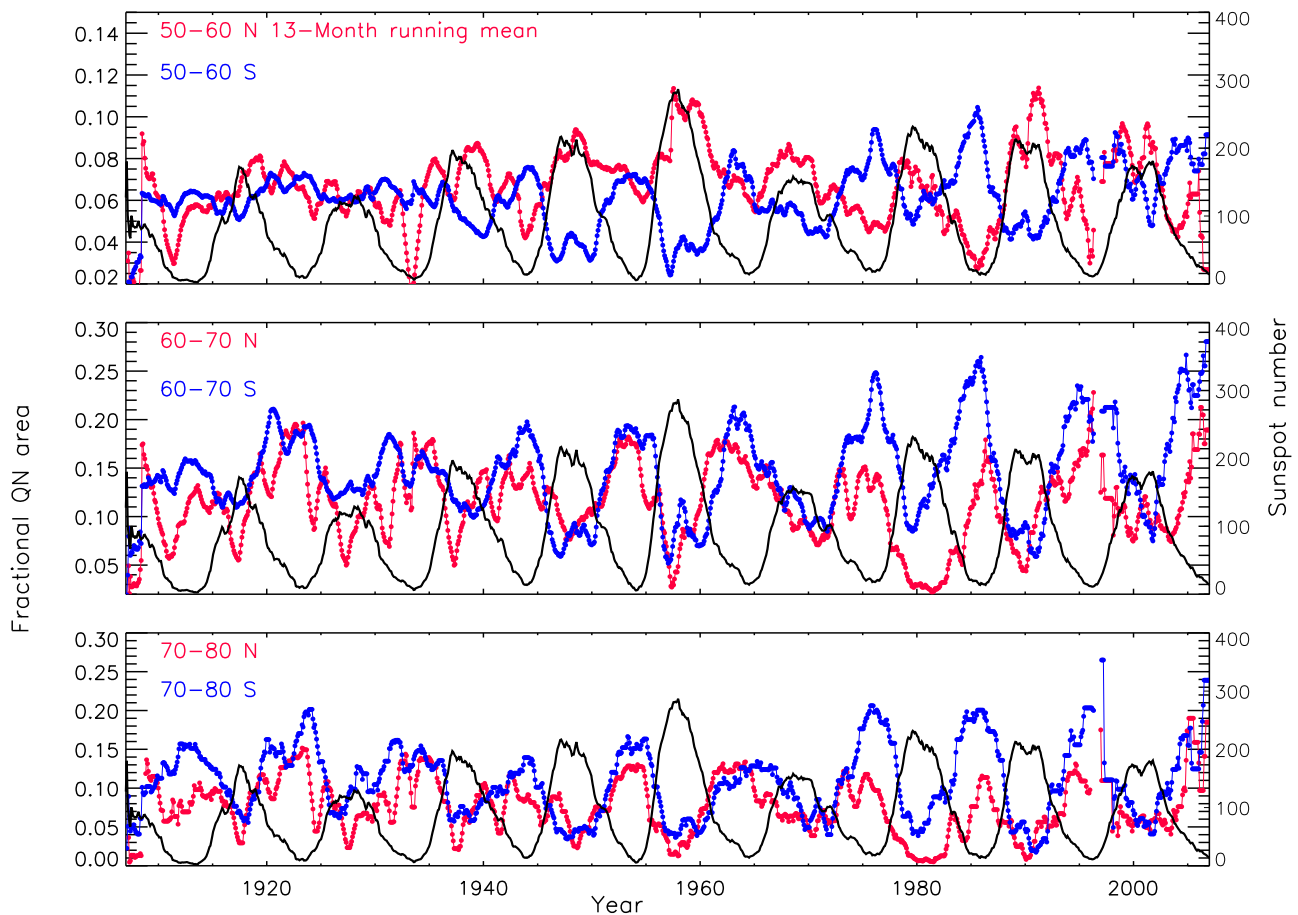


Figure A6. Same as for Figure A2, but for the fractional QN area.

## Appendix B

### Phase Difference between Activity at Different Latitudes for Individual Solar Cycle

We have also computed the phase difference in the activity between the latitude belts for each solar cycle to determine its relation with the strength of the solar cycle. To determine the speed of the activity shift for the individual cycle, we selected the data of 16 yr centered on the maximum phase of each cycle, as listed in Table B1. The cross-correlation values for each data set representing cycle numbers 15–21 were computed. Figure B1 shows the cross-correlation curves between different latitude

belts ( $5^\circ$  to  $75^\circ$ ) and  $35^\circ$  belt for the EN area of solar cycle 19 for the two hemispheres. We list the phase-difference values for the EN and AN for various latitudes in the northern hemisphere with respect to the  $35^\circ$  latitude belt in Table B1 and for the southern hemisphere in Table B2 for individual cycles. “NSP” in the tables indicates that the respective cross-correlation curve has no significant peak. The phase differences for the plage area are computed only up to  $45^\circ$  and for other features up to  $75^\circ$ . The values indicate that the activity shifts from the midlatitude belt to lower-latitude belts at a faster rate at the beginning of the cycle than near the end of the solar cycle for all the analyzed data.

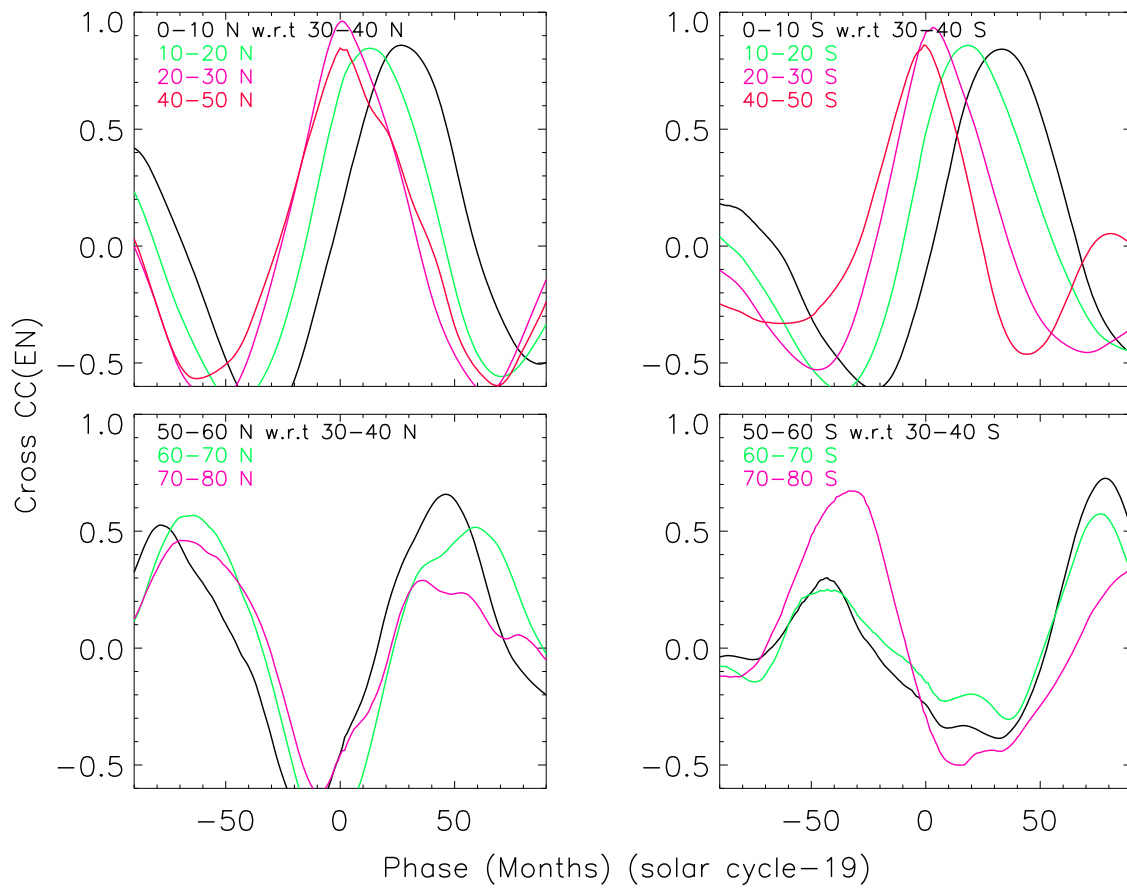


**Figure B1.** Cross-correlation curves for various latitude belts with respect to the 35° latitude belt for the EN area for solar cycle 19 considering the data for the period of 1952–67.

**Table B1**  
Phase Difference in Months between the Activity at Various Latitude Belts with Respect to the 35° Belt for the Northern Hemisphere

Cycle Number	Period	5°	15°	25°	45°	55°	65°	75°
EN Area								
15	1910-25	36	17	4	-4	NSP, 56	NSP,58	NSP, 58
16	1921-36	42	22	2	-6	-32, NSP	-34, NSP	-42, NSP
17	1931-46	29	11	3	-2	NSP	NSP	NSP
18	1941-56	36	20	2	-2	-34, 82	-38, 80	-40, 81
19	1952-67	28	14	2	0	-78, 46	-65, 50	-63, 55
20	1962-77	31	16	4	-3	-47, 72	-53, 69	-44, 75
21	1973-84	37	18	4	-5	-55, 75	-56, 77	-58, 70
AN Area								
15	1910-25	31	17	4	NSP	-38, 57	-32, 60	-24, 65
16	1921-36	41	23	2	-5	-47, NSP	-47, NSP	-43, NSP
17	1931-46	31	11	2	0	NSP	NSP	NSP
18	1941-56	32	14	2	0	-38, 82	-40, 81	-36, 83
19	1952-67	29	12	2	1	-77, 47	-60, 62	-58, NSP
20	1962-77	30	16	4	-4	-47, 70	-50, 72	-42, 76
21	1973-84	32	13	3	-5	-61, NSP	-61, NSP	-58, NSP

**Note.** “NSP” indicates when no significant peak is found in the cross-correlation curve.



**Table B2**

Phase Difference in Months between the Maximum Activity at Various Latitude Belts with Respect to the 35° Belt for the Southern Hemisphere

Cycle Number	Period	5°	15°	25°	45°	55°	65°	75°
EN Area								
15	1910-25	39	25	3	0	NSP,69	NSP, 67	NSP, 66
16	1921-36	30	10	3	-3	NSP	NSP	NSP
17	1931-46	42	21	6	-2	NSP	NSP	NSP
18	1941-56	32	18	5	-2	-26, NSP	-16, NSP	-30, NSP
19	1952-67	34	20	4	-3	-43, 80	-42, 76	-33, NSP
20	1962-77	35	21	2	-2	-49, NSP	-50, NSP	NSP
21	1973-84	28	15	3	-1	NSP	-34, 63	-34, 78
AN Area								
15	1910-25	38	22	5	-1	-61, 64	-59, 65	-58, 67
16	1921-36	35	12	3	0	NSP	NSP	NSP
17	1931-46	39	21	5	-2	NSP	NSP	NSP
18	1941-56	30	15	1	-1	-33, NSP	-33, NSP	-35, NSP
19	1952-67	31	15	3	-2	NSP	NSP	NSP
20	1962-77	33	15	0	-2	-53, NSP	-51, NSP	-37, NSP
21	1973-84	26	13	4	0	NSP	NSP	NSP

**Note.** “NSP” indicates when no significant peak is found in the cross-correlation curve.

### Appendix C

#### Phase Difference between the Activity at Different Latitudes and Sunspot Number

We have also analyzed the data for the individual solar cycles. Figure C1 shows the representative cross-correlation

curves for the EN area for solar cycle 19, considering the data for the period 1952–67. We list the values of phase difference for the EN and AN with sunspot numbers for various latitudes for the northern hemisphere in Table C1 and for the southern hemisphere in Table C2 for individual cycles. “NSP” in the

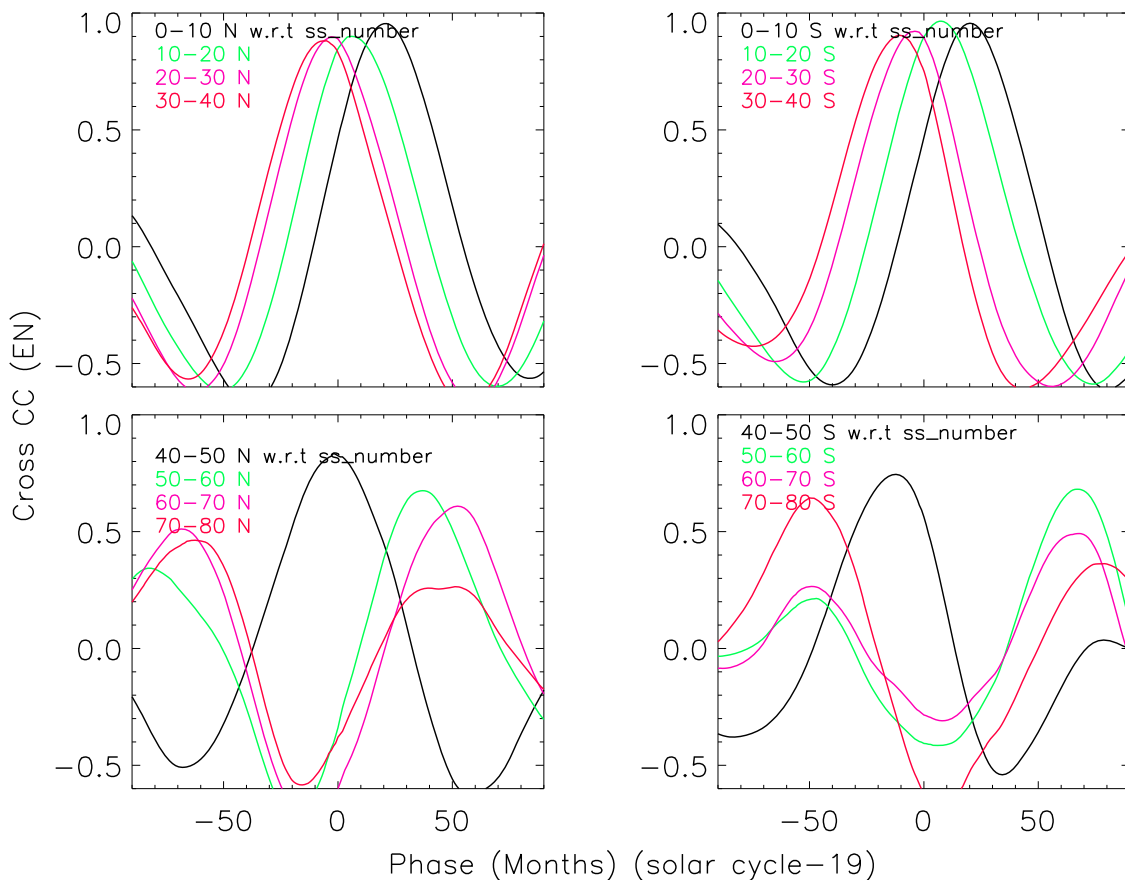


**Figure C1.** Cross-correlation curves of the Ca-K EN area for 5°, 15°, 25°, 35°, and 45° latitude belts with respect to SS over the visible disk considering the data period of 1952–67, representing the analysis for solar cycle 19.

**Table C1**

Phase Difference in Months between the Maximum Activity at Various Latitude Belts with Respect to Sunspot Number for the Northern Hemisphere for Each Solar Cycle

Cycle Number	Period	5°	15°	25°	35°	45°	55°	65°	75°
EN Area									
15	1910-25	14	0	-8	-14	-31,68	NSP, 45	NSP,48	NSP,52
16	1921-36	22	3	-4	-9	-19, NSP	-62, 81	-60, 80	-55, 83
17	1931-46	16	3	-2	-6	-7	-28, NSP	-37, NSP	NSP
18	1941-56	21	5	-2	-8	-12	-41, 65	-45, 62	-43, 64
19	1952-67	22	6	-2	-7	-2	-81, 37	-67, 54	-60, 49
20	1962-77	11	-2	-15	-23	-31	-72, 72	-71, 67	-67, 68
21	1973-83	18	2	-7	-14	-26	-76, 67	-78, 71	-74, 60
AN Area									
15	1910-25	13	0	-6	-13	NSP, 50	NSP, 46	NSP, 44	NSP, 51
16	1921-36	22	4	-5	-12	-52, NSP	-63, 82	-54, NSP	-48, 84
17	1931-46	17	3	-3	-7	NSP	NSP	NSP	NSP
18	1941-56	21	4	-4	-8	NSP	-41, 64	-45, 64	-44, 68
19	1952-67	21	5	-4	-8	0	-77, 40	-68, 56	NSP, 54
20	1962-77	11	-2	-15	-22	-55	-67, 72	-66, 71	-64, 68
21	1973-83	12	-3	-9	-14	-29	-75, 68	-77,72	-74, 60

**Note.** “NSP” indicates when no significant peak is found in the cross-correlation curve.

**Table C2**



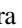

Phase Difference in Months between the Maximum Activity at Various Latitude Belts with Respect to sunspot Number for the Southern Hemisphere for Each Solar Cycle

Cycle number	Period	5°	15°	25°	35°	45°	55°	65°	75°
EN Area									
15	1910-25	23	8	-4	-15	-32, NSP	-43, 72	-60, 50	-69, 65
16	1921-36	19	2	-4	-8	-6	NSP	-57, 38	-48, 63
17	1931-46	19	5	-6	-14	-18	-25, NSP	-63, NSP	-60, NSP
18	1941-56	18	3	-4	-10	-16	-36, 81	-35, 75	-35, 73
19	1952-67	20	7	-5	-12	-13	-47, 67	-50, 65	-49, 78
20	1962-77	21	8	-6	-14	-22	-76, NSP	NSP	NSP, 82
21	1973-83	22	15	0	-6	-8	-38, NSP	-42, 48	-40, 72
AN Area									
15	1910-25	22	8	-4	-13	-29, NSP	NSP, 52	-63, 50	-64, 63
16	1921-36	21	4	-4	-8	NSP	NSP	-62, 40	-54, 65
17	1931-46	19	3	-6	-13	-18	-26, 75	-61, 67	-66, 65
18	1941-56	18	2	-4	-10	-20	-40, 75	-48, 72	NSP, 72
19	1952-67	20	6	-5	-10	-11	-54, 67	-52, 64	NSP
20	1962-77	22	8	-5	-12	-60	-71, NSP	-73, NSP	-44, NSP
21	1973-83	17	8	-4	-8	-9	NSP	-40, 49	-43, 69

**Note.** “NSP” indicates when no significant peak is found in the cross-correlation curve.

tables indicates that the respective cross-correlation curve has no significant peak.

### ORCID iDs

Muthu Priyal  <https://orcid.org/0000-0001-6093-3302>  
 Jagdev Singh  <https://orcid.org/0000-0003-0562-2979>  
 Belur Ravindra  <https://orcid.org/0000-0003-2165-3388>  
 G. Sindhuja  <https://orcid.org/0000-0002-5893-1938>

### References

- Ananthakrishnan, R. 1952, *Natur*, 170, 156  
 Babcock, H. W. 1961, *ApJ*, 133, 572  
 Belucz, B., Dikpati, M., & Forgács-Dajka, E. 2015, *ApJ*, 806, 169  
 Cameron, R., & Hopkins, A. 1998, *SoPh*, 183, 263  
 Charbonneau, P., Beaubien, G., & St-Jean, C. 2007, *ApJ*, 658, 657  
 Choudhuri, A. R., Schussler, M., & Dikpati, M. 1995, *A&A*, 303, L29  
 Devi, P., Singh, J., Chandra, R., Priyal, M., & Joshi, R. 2021, *SoPh*, 296, 49  
 Dikpati, M., & Gilman, P. A. 2006, *ApJ*, 649, 498  
 Dikpati, M., & Gilman, P. A. 2012, *ApJ*, 746, 65  
 Dikpati, M., Gilman, P. A., de Toma, G., & Ulrich, R. K. 2010, *GeoRL*, 37, L14107  
 Durrant, C. J., Turner, J. P. R., & Wilson, P. R. 2004, *SoPh*, 222, 345  
 Hale, G. E. 1908, *ApJ*, 28, 315  
 Hathaway, D. H. 2003, in Proc. of SOHO 12/GONG+ 2002. Local and Global Helioseismology: The Present and Future, ed. H. Sawaya-Lacoste (Noordwijk: ESA), 87  
 Hathaway, D. H., & Rightmire, L. 2010, *Sci*, 327, 1350  
 Howard, R., & Labonte, B. J. 1981, *SoPh*, 74, 131  
 Komm, R. W., Howard, R. F., & Harvey, J. W. 1993, *SoPh*, 147, 207  
 Leighton, R. B. 1959, *ApJ*, 130, 366

- Leighton, R. B. 1964, [ApJ](#), **140**, 1547
- Leighton, R. B. 1969, [ApJ](#), **156**, 1
- Makarov, V. I., Tlatov, A. G., & Callebaut, D. K. 2004, [SoPh](#), **224**, 49
- Nandy, D., Munoz-Jaramillo, A., & Martens, P. C. H. 2011, [Natur](#), **471**, 80
- Ortiz, A., & Rast, M. 2005, *Mem. Soc. Astron. Italiana*, **76**, 1018
- Priyal, M., Singh, J., Ravindra, B., & Shekar B, C. 2019, [SoPh](#), **294**, 131
- Rajaguru, S. P., & Antia, H. M. 2015, [ApJ](#), **813**, 114
- Raouafi, N. E., Harvey, J. W., & Henney, C. J. 2007, [ApJ](#), **669**, 636
- Schwabe, S. H. 1843, [AN](#), **20**, 283
- Sindhuja, G., Singh, J., & Priyal, M. 2015, [MNRAS](#), **448**, 2798
- Sindhuja, G., Singh, J., & Ravindra, B. 2014, [ApJ](#), **792**, 22
- Singh, J. 1988, *KodOB*, **9**, 159
- Singh, J., & Bappu, M. K. V. 1981, [SoPh](#), **71**, 161
- Singh, J., Gholami, I., & Muneer, S. 2004, [AdSpR](#), **34**, 265
- Singh, J., Priyal, M., & Ravindra, B. 2021, [ApJ](#), **908**, 210
- Singh, J., Priyal, M., Ravindra, B., Bertello, L., & Pevtsov, A. A. 2022, [ApJ](#), **927**, 154
- Sivaraman, K. R., & Livingston, W. C. 1982, [SoPh](#), **80**, 227
- Sivaraman, K. R., Singh, J., Bagare, S. P., & Gupta, S. S. 1987, [ApJ](#), **313**, 456
- Skumanich, A., Smythe, C., & Frazier, E. N. 1975, [ApJ](#), **200**, 747
- Wang, Y.-M., & Sheeley, N. R. 1988, [JGR](#), **93**, 11227
- White, O. R., & Livingston, W. C. 1981, [ApJ](#), **249**, 798
- Worden, J., & Harvey, J. 2000, [SoPh](#), **195**, 247
- Zhao, J., Bogart, R. S., Kosovichev, A. G., Duvall, T. L., & Hartlep, T. 2013, [ApJL](#), **774**, L29